Environmental Science Nano

PAPER

View Article Online
View Journal | View Issue

Cite this: *Environ. Sci.: Nano*, 2019, **6**, 3080

One-step sonochemical synthesis of a reduced graphene oxide – ZnO nanocomposite with antibacterial and antibiofouling properties†

Wei Zhang, [a] Yang Yang,[a] Eric Ziemann,[a] Avraham Be'er,[a] Muhammad Y. Bashouti, [b] Menachem Elimelech [c] and Roy Bernstein*[a]

Received 4th July 2019,
Accepted 21st August 2019

DOI: 10.1039/c9en00753a

rsc.li/es-nano

Microbial contamination and biofilm formation present major challenges in numerous applications. Many types of nanoparticles possess high antibacterial activity and thus are being investigated to combat environmental microbial contamination, limit bacterial deposition, and inhibit or destroy biofilms. In addition to finding nanoparticles with high and broad antibacterial activity, the synthesis of nanoparticles must also be sustainable and the nanoparticles should have low toxicity and low environmental impact. In this study, we developed a simple one-step probe sonication method to synthesize a ZnO nanoparticle functionalized reduced graphene oxide (rGO–ZnO) nanocomposite by exfoliating oxidized graphite in the presence of Zn^{2+}. The antibacterial activity of the nanocomposite was higher than that of graphene oxide (GO) and rGO against Gram-negative (*Escherichia coli* and *Serratia marcescens*) and Gram-positive (*Bacillus subtilis*) bacteria. Direct intracellular reactive oxygen species (ROS) and Zn^{2+} leaching measurements indicated that the high antibacterial activity against different bacteria of the nanocomposite arises from the formation of ROS, whereas the effect of Zn^{2+} is negligible. Furthermore, incorporating rGO–ZnO nanocomposite into a polyethersulfone (PES) membrane inhibited biofilm growth compared with a pristine PES membrane. Leaching experiments of Zn^{2+} from the incorporated rGO–ZnO membrane during synthetic wastewater filtration revealed that Zn^{2+} concentration in the effluent was below the environmental standards for potable and non-potable uses. Our research presents an effective, fast, and low-cost preparation method for developing nanocomposites with high antimicrobial activities. Also, it shows that a nanocomposite incorporated polymeric membrane can be safely applied for water and wastewater treatment with minimum environmental impact.

Environmental significance

Today, besides showing a high and broad antibacterial activity, antibacterial nanomaterials should be synthesized by a simple and safe method, without producing hazardous byproducts, and with minimal environmental impact when applied. We developed a reduced graphene oxide/ZnO nanocomposite meeting these criteria. The nanocomposite was synthesized using a green one-step sonochemical method under ambient conditions. Antibacterial activity against Gram-negative and Gram-positive bacteria was displayed. When incorporated into a polyethersulfone membrane, biofilm formation was inhibited. Zn^{2+} leaching during synthetic wastewater filtration using the incorporated membrane was below the standard levels for effluent reuse and discharge. In conclusion, the rGO–ZnO nanocomposite is a promising and safe nanomaterial to minimize membrane biofouling, a challenging problem in membrane technology for water and wastewater treatment.

[a] *Department of Desalination and Water Treatment, Zuckerberg Institute for Water Research, The Jacob Blaustein Institutes for Desert Research, Ben-Gurion University of the Negev, Sede-Boqer Campus, 84990, Israel.*
E-mail: royber@bgu.ac.il
[b] *Department of Solar Energy and Environmental Physics, The Swiss Institute for Dryland Environmental & Energy Research, The Jacob Blaustein Institutes for Desert Research, Ben-Gurion University of the Negev, Sede-Boqer Campus, 84990, Israel*
[c] *Department of Chemical and Environmental Engineering, Yale University, New Haven, CT 06520-8286, USA*

† Electronic supplementary information (ESI) available: Images of pristine PES membrane and rGO–ZnO (5% w/w) incorporated PES membrane (Fig. S1), the composition of synthetic wastewater for the Zn^{2+} leaching experiments (Table S1), TEM images for the rGO–ZnO composite at different magnifications (Fig. S2), Zn 2p HR-XPS spectra of ZnO nanoparticles and rGO–ZnO nanocomposite (Fig. S3), HR-XPS elemental composition results of GO, rGO and rGO–ZnO (Table S2), SEM images of *E. coli* following the contact killing assay on the surface of the uncoated and rGO–ZnO coated PES membrane (Fig. S4), a representative TEM image of a dead bacterium after the contact killing assay on rGO–ZnO coated PES membrane (Fig. S5), the MWCO and permeability (insert) of pristine PES membrane and rGO–ZnO incorporated PES membrane (Fig. S6), and the leaching behavior of Zn^{2+} from rGO–ZnO incorporated PES membrane (13.84 cm^2) during synthetic wastewater filtration (Fig. S7). See DOI: 10.1039/c9en00753a

1. Introduction

Bacterial contamination and biofilm formation are problems in many fields.[1,2] Consequently, there is intense interest in developing materials that kill bacteria and inhibit biofilm formation.[3] One promising, efficient strategy is the synthesis of antibacterial nanomaterials, including carbon-based materials.[4] Graphene, which is a carbon nanomaterial consisting of a two-dimensional sp^2-bonded monolayer, has attracted much attention in various fields due to its excellent electronic, mechanical, and thermal properties.[5,6] In particular, graphene oxide (GO), one of the most well-known, inexpensive graphene derivatives, exhibits bactericidal properties that arise from GO disrupting bacterial cell membranes on contact with its surface.[7–9] Therefore, GO has been widely researched for combating bacterial contamination and biofilm formation in many applications, including water treatment processes.[10–13] GO is also characterized by a large specific surface area and abundant functional groups (*e.g.*, epoxy, hydroxyl, and carboxyl groups), which endow GO with excellent hydrophilicity, dispersity, and biocompatibility.[14] The functional groups provide possible sites for hybridization and functionalization with other materials *via* covalent or physical interactions. This has inspired researchers to increase GO antimicrobial activity by synthesizing GO composites, such as metal oxide nanoparticle (NP)/GO composites (*e.g.*, GO/TiO_2, GO/CuO, and GO/Ag)[15–17] and metal–organic framework/GO composites.[18]

In addition to the requirement for high and broad antimicrobial activity, antimicrobial nanomaterials should also be environmentally friendly, have low toxicity, and use green synthesis methods.[19] Zinc oxide (ZnO) NPs, one of the biocompatible, low-toxicity, and affordable inorganic semiconductor metal oxides,[20,21] is considered such a type of material. ZnO NPs own broad antimicrobial activity against different microorganisms with or without UV/visible light.[22] The proposed mechanisms of ZnO antibacterial activity are the generation of reactive oxygen species (ROS),[23] release of zinc ions,[24] and internalization of NPs.[25] Based on these properties, GO/ZnO nanocomposite have been synthesized and studied for various applications. For example, Wang *et al.*[26] prepared the superior antibacterial ZnO/GO composites using the precipitation method. Wang *et al.*[27] immersed ZnO nanosheets in GO solution and used ultrasound to synthesize ZnO/GO composites for highly effective acetone vapor detection. More recently, Pruna *et al.*[28] obtained ZnO/GO hybrids by colloidal co-electrodeposition for use in methylene blue photocatalysis. Generally, graphene/ZnO nanocomposites are synthesized either by preparing each nanomaterial separately and combining them, or by preparing GO and then growing the ZnO NPs on the GO. In both types of synthesis, the ZnO NPs have been obtained by various methods, including sol–gel combustion,[29] chemical vapor deposition,[30] template-assisted growth,[31] and laser ablation and hydrothermal synthesis.[32,33] However, most of these technologies have drawbacks such as long reaction time, high temperature (>200 °C), complex apparatus, and the use or release of hazardous materials.

An efficient, simple, green alternative for preparing NPs and nanocomposite under ambient conditions is sonochemical synthesis. For instance, ZnO can be easily synthesized using the sonication method under alkaline conditions.[34] In addition, the synthesis of GO by the common modified Hummers method includes an exfoliation step of oxidized graphite, which is typically done by ultrasound. Furthermore, when the exfoliation is done under alkaline conditions, the GO deoxygenate to rGO, a less toxic form of graphene.[35,36] In this study, we combined the GO exfoliation step and conversion to rGO with synthesis of ZnO NPs and developed a facile one-step probe sonication method for synthesizing a nanocomposite of reduced graphene oxide (rGO) functionalized with ZnO NPs (rGO–ZnO) at ambient temperature under alkaline conditions. The incorporation of ZnO into rGO improved the antibacterial properties of the nanomaterials against both Gram-negative and Gram-positive bacteria. In addition, impregnating a polyethersulfone (PES) membrane with rGO–ZnO inhibited biofilm formation. The simple synthesis and high antibacterial activity against Gram-negative and Gram-positive bacteria of rGO–ZnO make it a promising material for surface antibiofilm modification in a range of applications.

2. Experimental section

2.1 Materials and chemicals

Graphite powder (200 mesh) was obtained from Alfa Aesar (UK). *N*-Methyl-2-pyrrolidone (NMP) was purchased from Carlo Erba (France). Luria broth (LB), agar, and glutaraldehyde solution (50% m/v in water) were purchased from Merck (USA). Sodium chloride (NaCl), potassium chloride (KCl), disodium phosphate (Na_2HPO_4), potassium dihydrogen phosphate (KH_2PO_4), and sodium hydroxide (NaOH) were obtained from Bio-Lab (Israel). SYTO-9, propidium iodide (PI), and concanavalin A were purchased from Life Technologies (USA) for performing live/dead cell assays and fluorescence imaging of extracellular polysaccharides (EPS), respectively. Zinc nitrate hexahydrate ($Zn(NO_3)_2{\cdot}6H_2O$), uranyl acetate, and 2′,7′-dichlorofluorescin diacetate (H_2DCF-DA) were obtained from Sigma-Aldrich (USA). All experiments were done with Milli-Q water (Millipore, USA).

2.2 Synthesis of GO, rGO, rGO–ZnO and ZnO

Unexfoliated GO nanosheets were synthesized and purified using the first step of the modified Hummers method followed by dialysis (3500 Da) for a week in water to remove the remaining metal species.[7] The unexfoliated GO was added to 0.1 M zinc nitrate solution (30 mL) to obtain a 1.5 mg mL^{-1} GO suspension, and the pH was adjusted to ~6 using 0.01 M NaOH. The suspension was left for 3 h to allow physical or chemical adsorption of the Zn^{2+} to the GO. The pH of the mixture was increased to 12 and the mixture was probe sonicated (VCX 130, Sonics, USA) for 120 min at 130 W

(45 s on and 15 s off) in an ice bath to synthesize the rGO–ZnO nanocomposite. At the end of the sonication, the suspension was purified by dialysis (3500 Da) in water for a week to remove traces of leached Zn^{2+} and base until the pH of the solution was ~7. The suspension was kept at room temperature until use. Exfoliated GO and rGO suspensions (1.5 mg mL^{-1}) were also prepared using the same procedure but without the addition of Zn^{2+} in Milli-Q water (GO) and alkaline solution (rGO), respectively. In addition, the ZnO NPs were prepared using the sonochemical method as the rGO–ZnO nanocomposite, but without GO.

2.3 Characterization of GO, rGO, rGO–ZnO and ZnO

The distribution of ZnO NPs on the rGO surface was investigated by transmission electron microscopy (TEM; Tecnai T12 G^2 TWIN, FEI Company, USA) with an acceleration voltage of 120 kV. The TEM sample was prepared by dropping the diluted (1 : 1000) rGO–ZnO suspension onto a lacey carbon grid surface. The nanocomposite was also characterized by X-ray diffraction (XRD; Panalytical B.V., Almelo, Netherland) equipped with a position-sensitive detector (X'Celerator, Malvern PANalytical). Data were collected in the $q/2q$ geometry using Cu Kα radiation (λ = 1.54178 Å) at 40 kV and 30 mA. Scans were run for ~15 min in a 2θ range of 5–60° at steps of ~0.033°. High-resolution X-ray photoelectron spectroscopy (XPS; ESCALAB 250, Thermo Fisher Scientific, USA) was performed with a monochromator and Al X-ray source. All spectra were calibrated relative to the C 1s peak at 284.5 eV.

2.4 Antibacterial activity

2.4.1 Contact killing assay. A single bacterial colony (*E. coli*, *B. subtilis*, *S. marcescens*, or *Staphylococcus aureus* (*S. aureus*)) was inoculated into 2 mL sterile LB broth and grown at 30 °C overnight. The bacterial suspension (0.1 mL) was transferred into fresh sterile LB broth (10 mL) and grown for another 3–5 h to reach the exponential phase (OD ≈ 1600 nm). Subsequently, the bacterial pellets were harvested and washed twice by centrifugation (6000 rpm, 1 min) using sterile phosphate-buffered saline (PBS) solution (~10 mM). Serially diluted bacterial culture (100 μL, ~10^6 CFU mL^{-1} in PBS) was added to an uncoated pristine or vacuum filtration coated (with GO, rGO or rGO–ZnO) 150 kDa PES membrane surface (1.13 cm^2, $n \geq 3$) for 3 h at room temperature in a biological hood (the coupons were placed in an empty Petri dish that was covered to avoid evaporation). After 3 h, the membrane coupon covered with 100 μL bacterial suspensions was carefully transferred to an Eppendorf tube containing PBS solution (0.9 mL) and vigorously shaken for 30 s. A sample of the diluted solution (100 μL) was spread on an LB agar plate and incubated at 30 °C overnight, and bacterial colonies that grew were counted. The experiments were repeated at least three times.

2.4.2 Bacterial morphology. The morphology of *E. coli* following the contact killing assay was visualized using scanning electron microscopy (SEM) and TEM. The contact killing assay was performed as described above, but with ~10^7 CFU mL^{-1} in PBS. For SEM, after the 3 h contact killing the culture was fixed by adding 2.5% (w/w) glutaraldehyde (100 μL) at 4 °C and was left undisturbed overnight. The membranes were gently washed twice with PBS solution and stained with osmium tetroxide (100 μL, 1% w/v). Gradient dehydration was performed using different ethanol solutions (25%, 50%, 75%, 90%, and 100% v/v) for 10 min each. Finally, the air-dried membrane was coated with gold *via* a sputter coater (Quorum Q150T-ES, Emitech, France) and observed by SEM (JSM-7400F, JEOL, Japan). For the TEM imaging, the bacteria were removed from the membranes as described above and put on a lacey F/C on Cu TEM grid (PELCO NetMesh 300, Ted Pella, USA), stained with uranyl acetate (2.5 μL, 0.5% w/v) for 30 s, dried, and imaged.

2.5 Antibacterial mechanisms

2.5.1 Oxidative stress mechanism. The ROS concentration in the *E. coli* cells was evaluated using H_2DCF-DA. An *E. coli* suspension (1 × 10^8 CFU mL^{-1} in LB, OD ≈ 1) was washed with 10 mM PBS solution. An absolute ethanol solution of 1 mM H_2DCF-DA (50 μL) was added to the bacterial suspension (0.95 mL in PBS) and the mixture was placed in an incubator (30 °C and 200 rpm) for 30 min. The stained bacteria were washed by centrifugation and re-dispersed in PBS. The stained bacterial PBS suspension (100 μL) and NP solution (100 μL; GO or rGO–ZnO) were put into a 96-well plate and the fluorescence intensity of each plate was automatically recorded every 20 min using a microplate reader (Infinite M200, Tecan, Switzerland) at 30 °C and 530 nm with an excitation wavelength of 480 nm.

2.5.2 Zn^{2+} leaching evaluation. In order to mimic the contact killing experiment, 1 mL PBS solution was placed on rGO–ZnO nanocomposite coated membrane (11.34 cm^2) surface for 3 h. After that, the solution was filtered with a 0.22 μm membrane (Durapore, Millipore) and the leached Zn^{2+} concentration in the solution was measured with an inductively coupled plasma-optical emission spectrometer (ICP-OES, 720ES, Varian).

2.6 The properties of rGO–ZnO incorporated PES membrane

2.6.1 Preparation of rGO–ZnO incorporated PES membrane. PES membrane (15 wt% PES in NMP) and rGO–ZnO incorporated PES membrane (5% w/w rGO–ZnO) were fabricated *via* the phase immersion inversion method, as described before.[37] For the latter, before mixing the rGO–ZnO nanocomposite with the PES, they were centrifuged, washed and re-dispersed in NMP. The pristine PES membrane turning from white to brown demonstrated the successful incorporation of rGO–ZnO NPs into the PES membrane matrix (Fig. S1†). The membrane permeability and molecule weight cut off (MWCO) were measured using a dead-end stirred cell (Amicon 8050, Millipore, USA) filtration system.[38] The hydrophilicity of the membranes was also checked by measuring the contact angle using the sessile drop method.[39]

2.6.2 Biofilm formation in a flow cell. The biofilm formation on the pristine PES and rGO–ZnO incorporated PES membranes was evaluated using a custom-made flow cell employing *Pseudomonas aeruginosa* (*P. aeruginosa*), a well-known and investigated biofilm-forming bacterium as a model bacteria, as described previously.[40] One coupon from each membrane (1 × 1 cm) was glued to a glass slide with double-sided tape and the slide was placed vertically in the cell. The flow cell was washed with 70% (v/v) ethanol and with Milli-Q water several times. *P. aeruginosa* bacterial suspension (60 mL, ~10^7 CFU mL^{-1} in PBS solution) was passed through the flow cell using a peristaltic pump (2 mL min^{-1}) for the initial deposition of the cells, followed by 10% LB solution (containing 0.9% NaCl) at room temperature for biofilm growth. After 36 h, the membranes were removed, gently rinsed with 10 mM PBS solution, and immediately stained with SYTO 9, PI, and concanavalin A for live bacteria, dead bacteria, and extracellular polymeric substances (EPS), respectively, for 20 min in a dark environment. The biofilm formed on the membrane surface was measured and analyzed (dead/live cell and EPS biovolume) using a previously reported procedure.[41]

2.6.3 Leaching of Zn^{2+} to the environment. Zn^{2+} leaching from the rGO–ZnO incorporated PES membrane to the environment was evaluated during filtration of synthetic wastewater. The composition of the synthetic wastewater is given in Table S1.† The synthetic wastewater was filtered using a dead-end filtration system described in our previous work at constant pressure (applied pressure ~0.7 bars).[41] Samples were collected during the filtration process at different permeate volumes until a total volume of 2 L was collected. The Zn^{2+} concentration was measured using ICP as described above.

2.7 Statistical analyses

Statistical analyses were conducted *via* one-way analysis of variance (ANOVA) followed by the *post hoc* test (Tukey HSD) using Origin software (Origin Lab, USA).

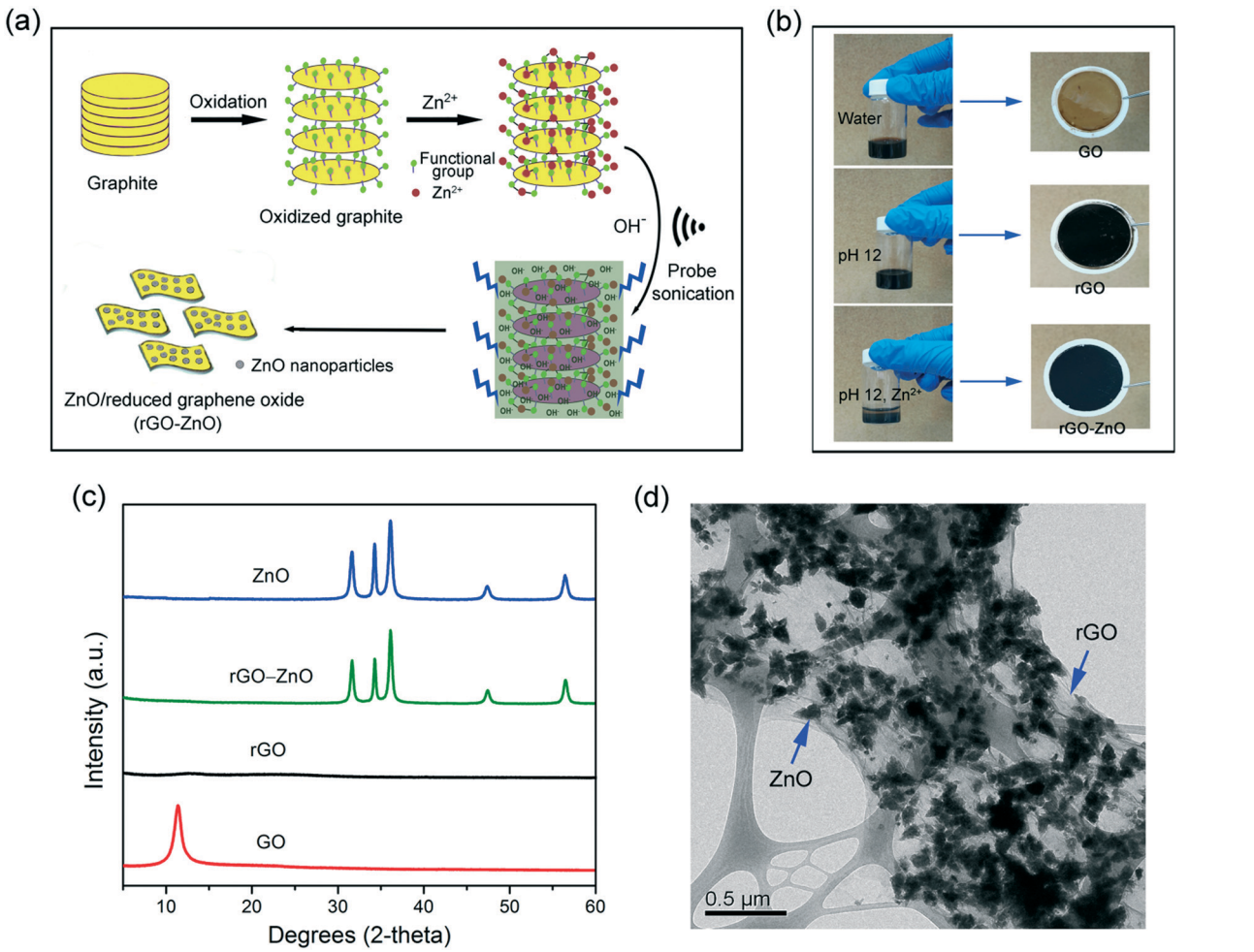

Fig. 1 (a) Proposed mechanism for the synthesis of rGO nanosheets functionalized with ZnO NPs. (b) Photographs of the GO, rGO, and rGO–ZnO suspensions and the corresponding 150 kDa PES membranes coated with nanomaterials by vacuum filtration. (c) XRD patterns of GO, rGO, rGO–ZnO and ZnO. (d) A representative TEM micrograph of rGO–ZnO on the carbon-coated grid.

3. Results and discussion

3.1 Preparation and characterization of rGO–ZnO

Fig. 1a describes the proposed mechanism for the formation of rGO–ZnO nanocomposite by one-step probe sonication method. First, oxygen-containing functional groups are introduced on the surfaces and edges of the graphite during the chemical oxidation process.[42] These oxygen-containing groups can act as anchor sites for the adsorption of Zn^{2+}, which eventually form ZnO NPs during the exfoliation step using probe sonication. Fig. 1b shows the images of prepared NPs solution following the sonication step and 150 kDa PES membranes coated with NPs by vacuum filtration. As seen, GO and rGO without Zn^{2+} formed stable suspensions, whereas exfoliation under alkaline conditions with Zn^{2+} resulted in the precipitation of the NPs. The GO coated membrane was yellow, whereas the membranes that were coated with NPs exfoliated at pH 12 (with and without Zn^{2+}) were black. The color change from yellow to black confirmed the formation of rGO probably as a result of deoxygenation of GO under alkaline conditions.[43] The precipitation of rGO with the addition of Zn^{2+} suggested that the rGO–ZnO nanocomposite was produced.

XRD analysis of GO, rGO, rGO–ZnO, and ZnO was performed to confirm the formation of crystalline ZnO NPs in the rGO–ZnO nanocomposite. As shown in Fig. 1c, the GO spectrum contained a diffraction peak around 11.45°, assigned as the characteristic GO oxidation peak.[44] This peak did not appear in the rGO and rGO–ZnO spectra, indicating that GO was converted to rGO by deoxygenation under the alkaline probe sonication conditions without Zn^{2+}. The spectrum of the rGO–ZnO nanocomposite contained five new characteristic diffraction peaks that were assigned to ZnO (2θ = 31.57°, 34.31°, 36.09°, 47.42°, and 56.44°, JCPDS 36-1451)[45,46] and indicate the synthesis of the rGO–ZnO nanocomposite. The distribution of ZnO NPs on rGO and the ZnO NP size were further determined by TEM. The TEM images show that ZnO NPs (~20–50 nm) were distributed at a high concentration on the rGO surface (Fig. 1d and S2†).

The chemical compositions of GO, rGO, and rGO–ZnO were measured by XPS (Fig. 2 and Table S2†). In the wide-scan XPS spectra (Fig. 2a), the carbon fraction (~284.81 eV)

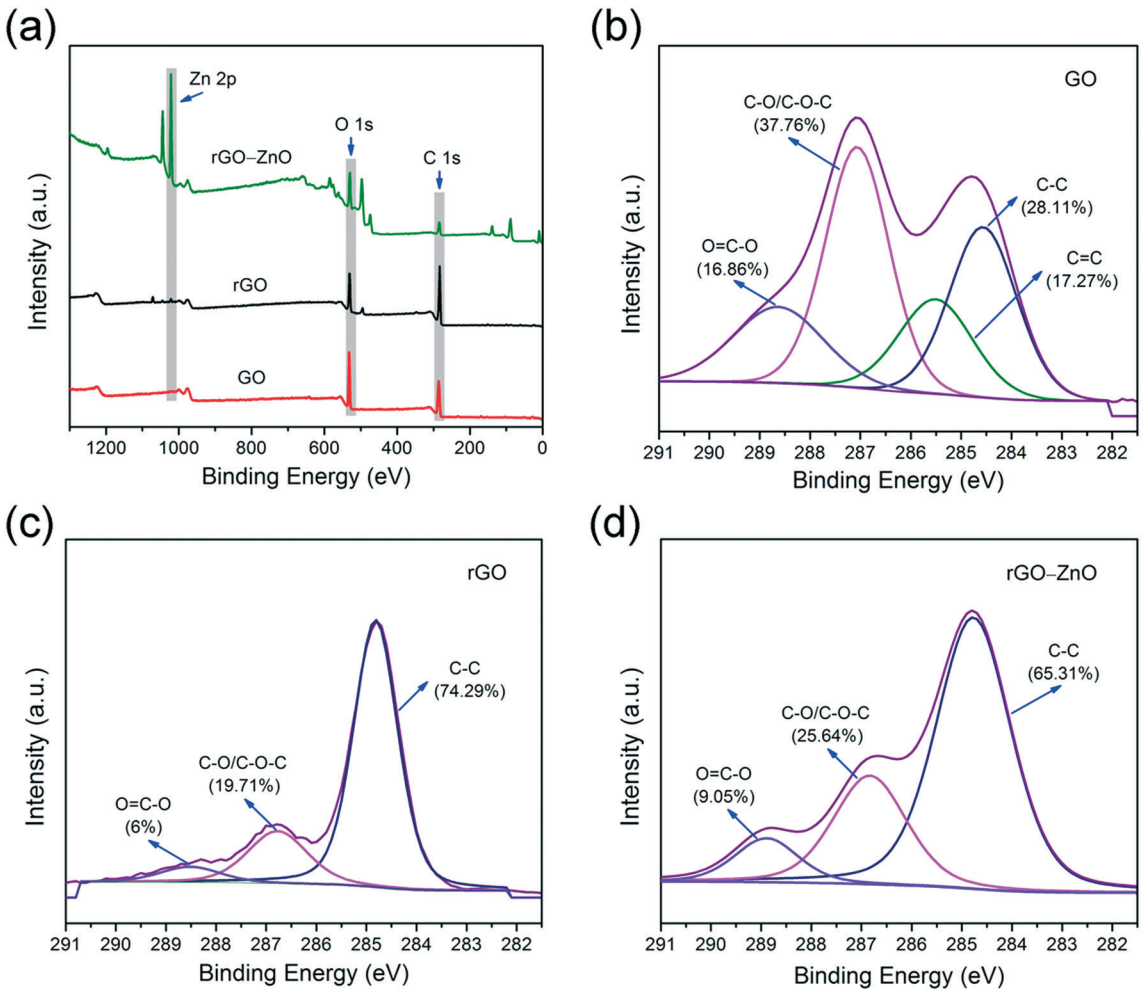

Fig. 2 (a) Wide-scan XPS survey and C 1s high-resolution XPS spectra of (b) GO, (c) rGO, and (d) rGO–ZnO. The corresponding deconvoluted curves are associated with different carbon-containing groups in each sample.

of rGO increased compared with GO, whereas the oxygen fraction (~532.35 eV) decreased due to the deoxygenation of GO. In addition, a new Zn 2p peak (centered at 1022.02 eV) appeared in the rGO–ZnO spectrum. High-resolution XPS of the Zn 2p revealed a positive shift in the binding energy (Δ = 0.76 eV) between pure ZnO NPs and rGO–ZnO (Fig. S3†), indicating a strong interaction between ZnO and rGO.[47] High-resolution XPS of the C 1s peak further showed differences in the carbon compositions of GO, rGO and rGO–ZnO. The C 1s spectrum of GO (Fig. 2b) contained four carbon peaks at 284.56, 285.51, 287.06, and 288.63 eV, corresponding to C–C, C═C, C–O/C–O–C, and O═C–O, respectively.[48] In the rGO spectrum (Fig. 2c), the C═C peak disappeared, the concentration of O═C–O and C–O carbon-containing functional groups decreased, and the C–C peak increased compared with these peaks in GO (Table S2†). Similar to rGO, the C═C peak disappeared in the rGO–ZnO spectrum (Fig. 2d). Moreover, rGO–ZnO had fewer O═C–O and C–O carbon-containing functional groups than GO (Table S2†). These findings demonstrate that GO was reduced to rGO by deoxygenation during preparation of the nanocomposite.

3.2 Antibacterial activity

Surface contact killing experiments were performed on pristine and NPs coated 150 kDa PES membranes (the PES membrane here is simply acted as a support for the NPs). As shown in Fig. 3, compared with the pristine membrane (control), the number of *E. coli* colonies decreased by ~15% for the rGO coated membrane, ~40% for the GO coated membrane, and ~95% for the rGO–ZnO coated membrane. Moreover, it could be clearly notice that the bactericidal activity of rGO–ZnO nanocomposite was also high (≥95%) against *S. marcescens* (Gram-negative) and *B. subtilis* (Gram-positive)

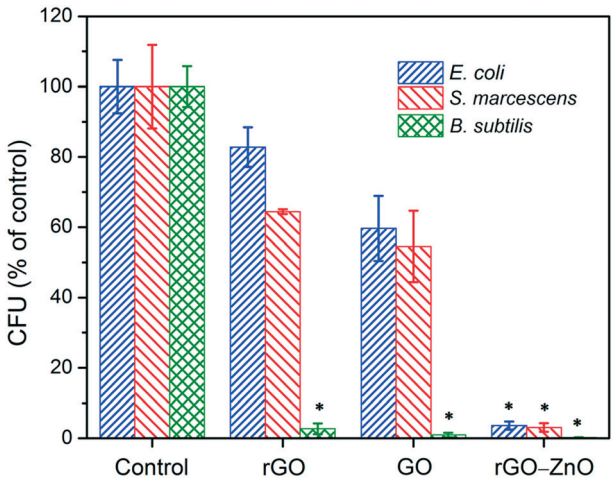

Fig. 3 Contact killing activity of rGO, GO, and rGO–ZnO nanocomposite on the PES membrane surface (1.13 cm^2) against *E. coli*, *S. marcescens* and *B. subtilis* (100 μL, ~10^6 CFU mL^{-1} in PBS). The values are expressed as means ± SD, $n \geq 4$. The asterisk indicates that the difference of its antibacterial property was statistically significant ($p < 0.05$) compared to control.

(and same as with the *E. coli*, much higher than the antibacterial activity of the rGO and GO), further demonstrating that the rGO–ZnO nanocomposite has high antibacterial activity against Gram-negative and Gram-positive bacteria. However, the rGO–ZnO coated PES membrane had insignificant contact killing activity for *S. aureus* (less than 10% reduction). The stability of *S. aureus* to antibacterial NPs and specifically to ZnO was reported by Ann *et al.*,[49] who attributed this property to the ability of *S. aureus* to build an effective shield against oxidative stress caused by ZnO NPs, by releasing responsive gene products.

To confirm the antibacterial activity of the rGO–ZnO nanocomposite qualitatively and visually, the bacterial morphology after 3 h surface contact killing was further imaged by SEM. All *E. coli* cells on the surface of the uncoated membrane were smooth and intact (Fig. 4a–c and S4a and b†). Conversely, the integrity of most cells on the rGO–ZnO coated membrane was compromised and cells appeared disintegrated and flattened (red arrows in Fig. 4d–f and S4d†). This indicates that the rGO–ZnO nanocomposite indeed effectively suppressed the bacteria viability. TEM analysis also showed the damaged bacterial structure and cell debris after contact with the rGO–ZnO coated membrane (Fig. 4g and h and S5†). As seen, the bacteria on the uncoated membrane remained intact (Fig. 4g), whereas the bacteria on the rGO–ZnO coated membrane were damaged (Fig. S5†) or completely destroyed (Fig. 4h).

3.3 Antibacterial mechanisms of rGO–ZnO

The oxidative stress induced by ROS generation is usually considered one of the main antibacterial mechanisms for GO and ZnO NPs.[34,36] To assess the ROS formation by rGO–ZnO in *E. coli*, non-fluorescent H_2DCF-DA was used as an indicator. H_2DCF-DA easily penetrates the bacterial cell membrane and is hydrolyzed by intracellular esterases to nonfluorescent dihydrodichlorofluorescein (DCFH). In the presence of ROS, DCFH is oxidized to highly fluorescent dichlorofluorescein (DCF).[50] Thus, the ROS concentration in the bacteria cell is directly proportional to the fluorescent intensity of DCF. Fig. 5 shows the fluorescence intensity of GO and rGO–ZnO after 3 h contact with the bacteria solution. The higher fluorescence intensity of the rGO–ZnO solution compared to the GO solution suggests that the combination of ZnO NPs and rGO dramatically increase ROS generation. Applerot *et al.*[34] reported that a high concentration of ROS could be spontaneously generated at the ZnO NP surface and penetrated bacterial cells. In another study, Li *et al.*[51] showed that rGO decreased the recombination of highly activated electron–hole pairs generated at the ZnO NP surface. Thus, the combination of these two effects probably causes the high ROS formation by the nanocomposite, which is responsible for its high antibacterial properties against Gram-negative and Gram-positive bacteria.

In addition, it has also been reported that leaching of Zn^{2+} from ZnO is a main antibacterial mechanism of ZnO NPs.[24,52] Therefore, the concentration of Zn^{2+} leached from the rGO–

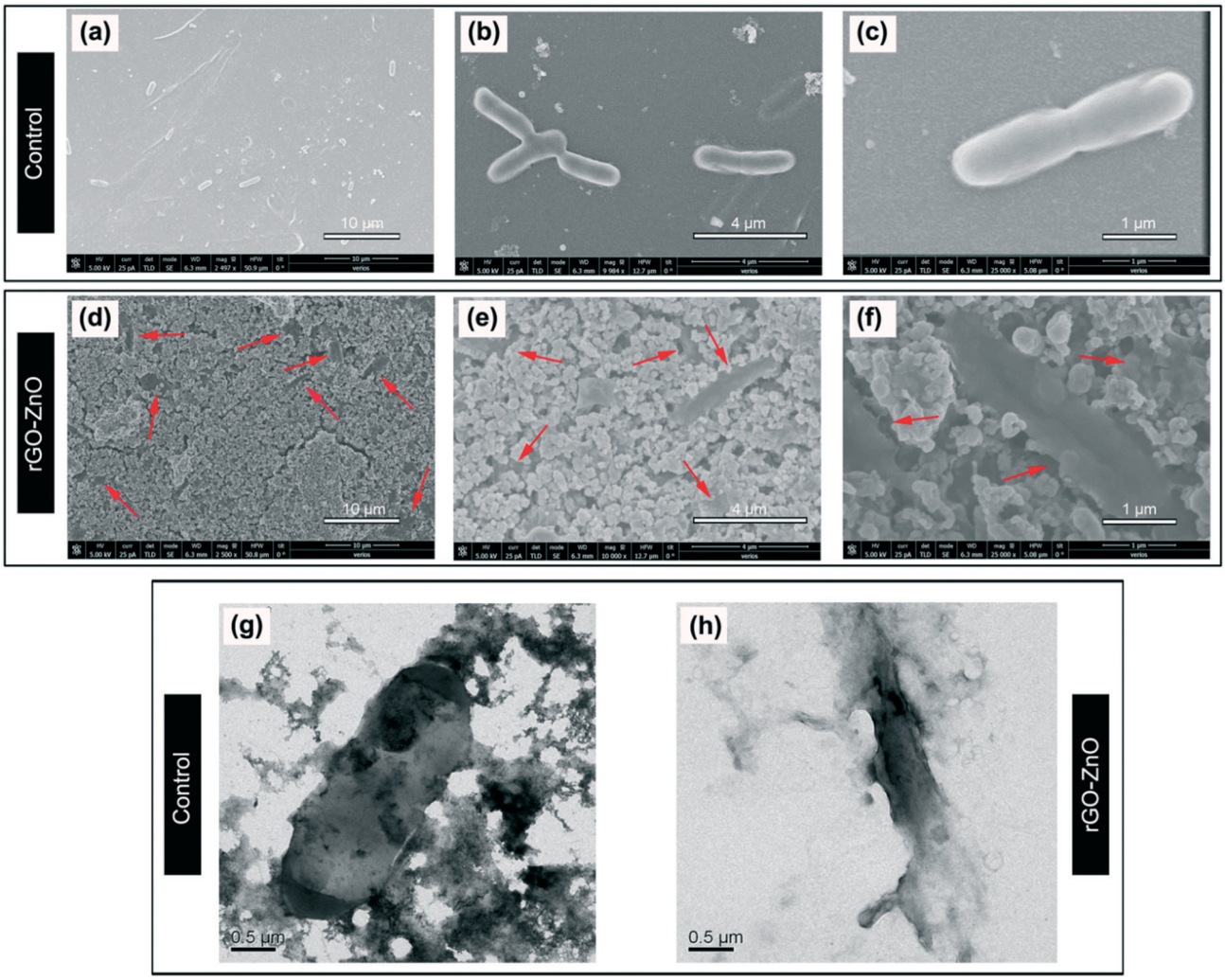

Fig. 4 (a–f) SEM and (g and h) TEM images of *E. coli* following the contact killing assay on the surface of the (a–c and g) uncoated and (d–f and h) rGO–ZnO coated PES membranes. The bacteria were stained with osmium tetroxide for SEM and uranyl chloride for TEM. Red arrows indicate damaged cells. The black spots in image g are uranyl acetate.

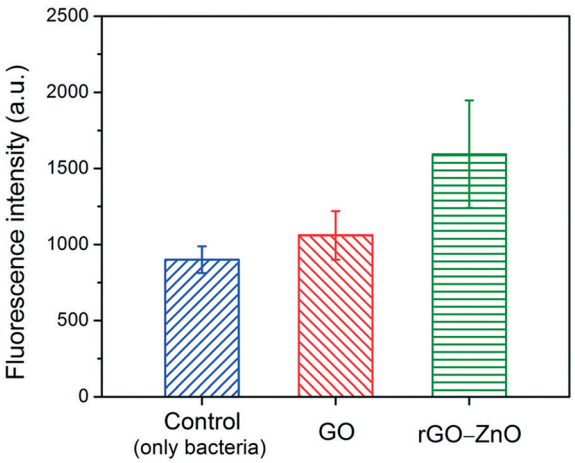

Fig. 5 DCF fluorescence intensity for *E. coli* cells in GO, rGO–ZnO and for pure bacteria solution, reflecting the amount of ROS generated. The values are expressed as means ± SD, n = 8.

ZnO coated PES membrane to the PBS solution under the similar conditions that were applied during the contact killing assay was further measured. We found that the leaching of rGO–ZnO in PBS solution after 3 h was ~0.7 mg L^{-1}. According to Franklin *et al.*,[53] in the antibacterial mechanism of ZnO NPs, free Zn^{2+} affect the bacterial viability only when the Zn^{2+} concentration is above 10 mg L^{-1}. Hence, it can be assumed that the antibacterial activity of rGO–ZnO is caused mainly by oxidative stress. Moreover, the low leaching of Zn^{2+} and the fact that the nanocomposite stored for more than one month had an antibacterial activity similar to that of the fresh nanocomposite, indicating that the rGO–ZnO nanocomposite is stable and has long-term antibacterial activity.

3.4 The properties of rGO–ZnO incorporated PES membrane

3.4.1 Antibiofouling behavior in flow-cell. Initial bacterial deposition is known to be the first stage of biofilm formation on surfaces such as polymeric membranes.[40,54] Therefore,

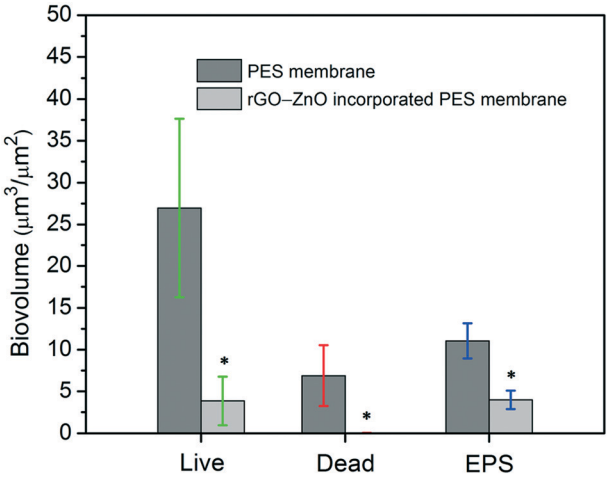

Fig. 6 Biofilm biovolume of live cells, dead cells, and EPS on pristine and rGO–ZnO incorporated PES membrane surfaces (5 wt% ZnO) after 36 h using *P. aeruginosa* as a model bacterium. The results are averages of two independent biofilm experiments with SD calculated from twenty random positions on each sample (n = 20). The asterisk indicates that the difference in biovolume of the live cells, dead cells, and EPS of the rGO–ZnO incorporated PES membrane was statistically significant ($p < 0.05$) compared with that of the pristine PES membrane.

incorporating antibacterial NPs into the membrane matrix might inhibit biofilm formation.[55] The antibiofouling activity of the rGO–ZnO nanocomposite was studied using pristine and rGO–ZnO incorporated PES membranes (the two membranes had a similar MWCO ~200 kDa and water permeability ~350 L m^{-2} h^{-1} bar^{-1}) (Fig. S6†) in a flow cell with *P. aeruginosa* as a model bacterium. As shown in Fig. 6, the rGO–ZnO incorporated PES membrane showed a significantly lower live and dead cell biovolume ($p < 0.05$) and much less EPS biovolume than the pristine PES membrane after 36 h. The lower level of biofilm formation on the incorporated membrane compared to the pristine one is probably attributable to proliferating bacteria deposited on the membrane surface being killed by the rGO–ZnO. This observation might also be attributed to fewer bacteria initially attached to the incorporated membrane surface due to the slightly increased hydrophilicity (67 ± 2°) compared with the pristine membrane (81 ± 3°). Nonetheless, a biofilm did form on the rGO–ZnO incorporated PES membrane, although it was much thinner than that on the pristine membrane. The antibiofouling activity could be further improved by increasing the nanocomposite concentration in the membrane, binding the NPs directly to the membrane surface,[56] or surface modification of the rGO–ZnO incorporated PES membrane with an antifouling coating to obtain dual antifouling and antibacterial properties.[41,57]

3.4.2 Leaching of Zn^{2+}. Leaching of Zn^{2+} from ZnO nanoparticles can have a negative environmental impact.[58] In addition, the presence of organic matter in water can also enhance the leaching of Zn^{2+}.[24] Therefore, Zn^{2+} leaching from the rGO–ZnO incorporated PES membrane was evaluated during filtration of synthetic wastewater. As seen in Fig. S7,† after a small amount of Zn^{2+} leached out from rGO–ZnO incorporated PES membrane at the beginning of the filtration, the Zn^{2+} concentration in the effluent significantly decreased with the filtered volume and was less than 50 μg L^{-1} between the first and the second liter filtered. This indicates that Zn^{2+} leaching from the rGO–ZnO incorporated PES membrane was very low. These concentrations are below the guidelines for generally non-potable use, such as irrigation,[59] aquifer recharge,[60] and effluent discharge.[61] It is also well below the standards for portable use in most countries (typically ≥1 mg L^{-1}).[62–64] The low leaching can be attributed to the stability of the ZnO NPs in the nanocomposite as was recently suggested,[65] and to the incorporation of the nanocomposite in the polymer matrix. Hence, we conclude that the rGO–ZnO incorporated PES membrane is stable and safe in the treatment of water and wastewater.

4. Conclusion

In this research, we synthesized the rGO–ZnO nanocomposite by a simple one-step sonochemical method. The nanocomposite displayed high antimicrobial activity against Gram-negative and Gram-positive bacteria, mainly through the oxidative stress mechanism. The incorporation of rGO–ZnO into the PES membrane partly inhibited the *P. aeruginosa* biofilm formation while the Zn^{2+} leaching from the membrane during wastewater filtration was below the guidelines for potable and non-potable uses. Our results indicate that the rGO–ZnO nanocomposite is promising as an antibacterial nanomaterial for the surface modification of various substrates to increase their antibacterial activity, effectively inhibit bacterial growth and biofilm formation.

Conflicts of interest

The authors declare no conflicts of interest.

Acknowledgements

We acknowledge financial support from the United States–Israel Binational Agricultural Research and Development Fund (BARD), Grant IS-4977-16. A. B. is thankful for partial support from The Israel Science Foundation, Grant No. 373/16. M. B. is supported by an MAOF Grant from the Council for Higher Education in Israel for new faculty members. W. Z. is supported by the Kreitman Negev Scholarship for Distinguished Ph.D. Students from BGU and a graduate fellowship from China Scholarship Council (No: 201808510146).

References

1 J. Song, F. Zhang, Y. Huang, A. A. Keller, X. Tang, W. Zhang, W. Jia and J. Santos, Highly efficient bacterial removal and disinfection by magnetic barium phosphate nanoflakes with embedded iron oxide nanoparticles, *Environ. Sci.: Nano*, 2018, **5**, 1341–1349.

2 O. Sánchez, Microbial diversity in biofilms from reverse osmosis membranes: A short review, *J. Membr. Sci.*, 2018, **545**, 240–249.
3 Y. Liu, L. Shi, L. Su, H. C. van der Mei, P. C. Jutte, Y. Ren and H. J. Busscher, Nanotechnology-based antimicrobials and delivery systems for biofilm-infection control, *Chem. Soc. Rev.*, 2019, **48**, 428–446.
4 X. Zeng, G. Wang, Y. Liu and X. Zhang, Graphene-based antimicrobial nanomaterials: rational design and applications for water disinfection and microbial control, *Environ. Sci.: Nano*, 2017, **4**, 2248–2266.
5 C. Rao, A. Sood, R. Voggu and K. Subrahmanyam, Some novel attributes of graphene, *J. Phys. Chem. Lett.*, 2010, **1**, 572–580.
6 X. Zhu, K. Yang and B. Chen, Membranes prepared from graphene-based nanomaterials for sustainable applications: a review, *Environ. Sci.: Nano*, 2017, **4**, 2267–2285.
7 F. Perreault, A. F. De Faria, S. Nejati and M. Elimelech, Antimicrobial properties of graphene oxide nanosheets: why size matters, *ACS Nano*, 2015, **9**, 7226–7236.
8 X. Lu, X. Feng, J. R. Werber, C. Chu, I. Zucker, J.-H. Kim, C. O. Osuji and M. Elimelech, Enhanced antibacterial activity through the controlled alignment of graphene oxide nanosheets, *Proc. Natl. Acad. Sci. U. S. A.*, 2017, **114**, E9793–E9801.
9 F. Zou, H. Zhou, D. Y. Jeong, J. Kwon, S. U. Eom, T. J. Park, S. W. Hong and J. Lee, Wrinkled surface-mediated antibacterial activity of graphene oxide nanosheets, *ACS Appl. Mater. Interfaces*, 2017, **9**, 1343–1351.
10 H. N. Nguyen, C. Chaves-Lopez, R. C. Oliveira, A. Paparella and D. F. Rodrigues, Cellular and metabolic approaches to investigate the effects of graphene and graphene oxide in the fungi Aspergillus flavus and Aspergillus niger, *Carbon*, 2019, **143**, 419–429.
11 H. N. Nguyen and D. F. Rodrigues, Chronic toxicity of graphene and graphene oxide in sequencing batch bioreactors: a comparative investigation, *J. Hazard. Mater.*, 2018, **343**, 200–207.
12 J. Fan, C. D. Grande and D. F. Rodrigues, Biodegradation of graphene oxide-polymer nanocomposite films in wastewater, *Environ. Sci.: Nano*, 2017, **4**, 1808–1816.
13 F. Perreault, H. Jaramillo, M. Xie, M. Ude, L. D. Nghiem and M. Elimelech, Biofouling mitigation in forward osmosis using graphene oxide functionalized thin-film composite membranes, *Environ. Sci. Technol.*, 2016, **50**, 5840–5848.
14 S. Stankovich, D. A. Dikin, R. D. Piner, K. A. Kohlhaas, A. Kleinhammes, Y. Jia, Y. Wu, S. T. Nguyen and R. S. Ruoff, Synthesis of graphene-based nanosheets via chemical reduction of exfoliated graphite oxide, *Carbon*, 2007, **45**, 1558–1565.
15 Y.-N. Chang, X.-M. Ou, G.-M. Zeng, J.-L. Gong, C.-H. Deng, Y. Jiang, J. Liang, G.-Q. Yuan, H.-Y. Liu and X. He, Synthesis of magnetic graphene oxide–TiO_2 and their antibacterial properties under solar irradiation, *Appl. Surf. Sci.*, 2015, **343**, 1–10.
16 Y. Li, D. Yang and J. Cui, Graphene oxide loaded with copper oxide nanoparticles as an antibacterial agent against Pseudomonas syringae pv. tomato, *RSC Adv.*, 2017, **7**, 38853–38860.
17 A. Soroush, W. Ma, Y. Silvino and M. S. Rahaman, Surface modification of thin film composite forward osmosis membrane by silver-decorated graphene-oxide nanosheets, *Environ. Sci.: Nano*, 2015, **2**, 395–405.
18 M. D. Firouzjaei, A. A. Shamsabadi, M. Sharifian Gh, A. Rahimpour and M. Soroush, A novel nanocomposite with superior antibacterial activity: a silver–based metal organic framework embellished with graphene oxide, *Adv. Mater. Interfaces*, 2018, **5**, 1701365.
19 M. S. Mauter, I. Zucker, F. Perreault, J. R. Werber, J.-H. Kim and M. Elimelech, The role of nanotechnology in tackling global water challenges, *Nat. Sustain.*, 2018, **1**, 166.
20 A. M. Díez-Pascual and A. L. Díez-Vicente, ZnO-reinforced poly (3-hydroxybutyrate-co-3-hydroxyvalerate) bionanocomposites with antimicrobial function for food packaging, *ACS Appl. Mater. Interfaces*, 2014, **6**, 9822–9834.
21 R. Saravanan, F. Gracia, M. M. Khan, V. Poornima, V. K. Gupta, V. Narayanan and A. Stephen, ZnO/CdO nanocomposites for textile effluent degradation and electrochemical detection, *J. Mol. Liq.*, 2015, **209**, 374–380.
22 V. Lakshmi Prasanna and R. Vijayaraghavan, Insight into the mechanism of antibacterial activity of ZnO: surface defects mediated reactive oxygen species even in the dark, *Langmuir*, 2015, **31**, 9155–9162.
23 A. R. Chowdhuri, S. Tripathy, S. Chandra, S. Roy and S. K. Sahu, A ZnO decorated chitosan–graphene oxide nanocomposite shows significantly enhanced antimicrobial activity with ROS generation, *RSC Adv.*, 2015, **5**, 49420–49428.
24 M. Li, L. Zhu and D. Lin, Toxicity of ZnO nanoparticles to Escherichia coli: mechanism and the influence of medium components, *Environ. Sci. Technol.*, 2011, **45**, 1977–1983.
25 R. Brayner, R. Ferrari-Iliou, N. Brivois, S. Djediat, M. F. Benedetti and F. Fiévet, Toxicological impact studies based on Escherichia coli bacteria in ultrafine ZnO nanoparticles colloidal medium, *Nano Lett.*, 2006, **6**, 866–870.
26 Y.-W. Wang, A. Cao, Y. Jiang, X. Zhang, J.-H. Liu, Y. Liu and H. Wang, Superior antibacterial activity of zinc oxide/graphene oxide composites originating from high zinc concentration localized around bacteria, *ACS Appl. Mater. Interfaces*, 2014, **6**, 2791–2798.
27 P. Wang, D. Wang, M. Zhang, Y. Zhu, Y. Xu, X. Ma and X. Wang, ZnO nanosheets/graphene oxide nanocomposites for highly effective acetone vapor detection, *Sens. Actuators, B*, 2016, **230**, 477–484.
28 A. Pruna, Z. Wu, J. Zapien, Y. Li and A. Ruotolo, Enhanced photocatalytic performance of ZnO nanostructures by electrochemical hybridization with graphene oxide, *Appl. Surf. Sci.*, 2018, **441**, 936–944.
29 X. Zhang, Y. Chen, S. Zhang and C. Qiu, High photocatalytic performance of high concentration Al-doped ZnO nanoparticles, *Sep. Purif. Technol.*, 2017, **172**, 236–241.
30 S. Vallejos, I. Gràcia, T. Lednický, L. Vojkuvka, E. Figueras, J. Hubálek and C. Cané, Highly hydrogen sensitive

micromachined sensors based on aerosol-assisted chemical vapor deposited ZnO rods, *Sens. Actuators, B*, 2018, **268**, 15–21.

31 C. Ou, P. E. Sanchez-Jimenez, A. Datta, F. L. Boughey, R. A. Whiter, S.-L. Sahonta and S. Kar-Narayan, Template-assisted hydrothermal growth of aligned zinc oxide nanowires for piezoelectric energy harvesting applications, *ACS Appl. Mater. Interfaces*, 2016, **8**, 13678–13683.

32 X. Wang, C. Xu, F. Qin, Y. Liu, A. Manohari, D. You, W. Liu, F. Chen, Z. Shi and Q. Cui, Ultraviolet lasing in Zn-rich ZnO microspheres fabricated by laser ablation, *Nanoscale*, 2018, **10**, 17852–17857.

33 W. Zhang, L. Meng, G. Mu, M. Zhao, P. Zou and Y. Zhang, A facile strategy for fabrication of nano-ZnO/yeast composites and their adsorption mechanism towards lead (II) ions, *Appl. Surf. Sci.*, 2016, **378**, 196–206.

34 G. Applerot, A. Lipovsky, R. Dror, N. Perkas, Y. Nitzan, R. Lubart and A. Gedanken, Enhanced antibacterial activity of nanocrystalline ZnO due to increased ROS–mediated cell injury, *Adv. Funct. Mater.*, 2009, **19**, 842–852.

35 M. Kryuchkova, A. Danilushkina, Y. Lvov and R. Fakhrullin, Evaluation of toxicity of nanoclays and graphene oxide in vivo: a Paramecium caudatum study, *Environ. Sci.: Nano*, 2016, **3**, 442–452.

36 S. Liu, T. H. Zeng, M. Hofmann, E. Burcombe, J. Wei, R. Jiang, J. Kong and Y. Chen, Antibacterial activity of graphite, graphite oxide, graphene oxide, and reduced graphene oxide: membrane and oxidative stress, *ACS Nano*, 2011, **5**, 6971–6980.

37 W. Zhang, Z. Yang, Y. Kaufman and R. Bernstein, Surface and anti-fouling properties of a polyampholyte hydrogel grafted onto a polyethersulfone membrane, *J. Colloid Interface Sci.*, 2018, **517**, 155–165.

38 M. Kaganovich, W. Zhang, V. Freger and R. Bernstein, Effect of the membrane exclusion mechanism on phosphate scaling during synthetic effluent desalination, *Water Res.*, 2019, **161**, 381–391.

39 A. D. Grossman, Y. Yang, U. Yogev, D. C. Camarena, G. Oron and R. Bernstein, Effect of ultrafiltration membrane material on fouling dynamics in a submerged anaerobic membrane bioreactor treating domestic wastewater, *Environ. Sci.: Water Res. Technol.*, 2019, **5**, 1145–1156.

40 R. Bernstein, V. Freger, J.-H. Lee, Y.-G. Kim, J. Lee and M. Herzberg, 'Should I stay or should I go?' Bacterial attachment vs biofilm formation on surface-modified membranes, *Biofouling*, 2014, **30**, 367–376.

41 W. Zhang, W. Cheng, E. Ziemann, A. Be'er, X. Lu, M. Elimelech and R. Bernstein, Functionalization of ultrafiltration membrane with polyampholyte hydrogel and graphene oxide to achieve dual antifouling and antibacterial properties, *J. Membr. Sci.*, 2018, **565**, 293–302.

42 J. Chen, Y. Li, L. Huang, C. Li and G. Shi, High-yield preparation of graphene oxide from small graphite flakes via an improved Hummers method with a simple purification process, *Carbon*, 2015, **81**, 826–834.

43 X. Fan, W. Peng, Y. Li, X. Li, S. Wang, G. Zhang and F. Zhang, Deoxygenation of exfoliated graphite oxide under alkaline conditions: a green route to graphene preparation, *Adv. Mater.*, 2008, **20**, 4490–4493.

44 W.-D. Yang, Y.-R. Li and Y.-C. Lee, Synthesis of rGO/TiO_2 composites via the UV-assisted photocatalytic reduction of graphene oxide, *Appl. Surf. Sci.*, 2016, **380**, 249–256.

45 V. Vaiano, M. Matarangolo, O. Sacco and D. Sannino, Photocatalytic treatment of aqueous solutions at high dye concentration using praseodymium-doped ZnO catalysts, *Appl. Catal., B*, 2017, **209**, 621–630.

46 G. Zhang, S. Hou, H. Zhang, W. Zeng, F. Yan, C. C. Li and H. Duan, High–Performance and Ultra–Stable Lithium–Ion Batteries Based on MOF–Derived ZnO@ZnO Quantum Dots/C Core–Shell Nanorod Arrays on a Carbon Cloth Anode, *Adv. Mater.*, 2015, **27**, 2400–2405.

47 X. Wu, L. Wen, K. Lv, K. Deng, D. Tang, H. Ye, D. Du, S. Liu and M. Li, Fabrication of ZnO/graphene flake-like photocatalyst with enhanced photoreactivity, *Appl. Surf. Sci.*, 2015, **358**, 130–136.

48 M. Velasco-Soto, S. Pérez-García, J. Alvarez-Quintana, Y. Cao, L. Nyborg and L. Licea-Jiménez, Selective band gap manipulation of graphene oxide by its reduction with mild reagents, *Carbon*, 2015, **93**, 967–973.

49 L. C. Ann, S. Mahmud, S. K. M. Bakhori, A. Sirelkhatim, D. Mohamad, H. Hasan, A. Seeni and R. A. Rahman, Antibacterial responses of zinc oxide structures against Staphylococcus aureus, Pseudomonas aeruginosa and Streptococcus pyogenes, *Ceram. Int.*, 2014, **40**, 2993–3001.

50 G. Applerot, J. Lellouche, A. Lipovsky, Y. Nitzan, R. Lubart, A. Gedanken and E. Banin, Understanding the antibacterial mechanism of CuO nanoparticles: revealing the route of induced oxidative stress, *Small*, 2012, **8**, 3326–3337.

51 B. Li, T. Liu, Y. Wang and Z. Wang, ZnO/graphene-oxide nanocomposite with remarkably enhanced visible-light-driven photocatalytic performance, *J. Colloid Interface Sci.*, 2012, **377**, 114–121.

52 J. Pasquet, Y. Chevalier, J. Pelletier, E. Couval, D. Bouvier and M.-A. Bolzinger, The contribution of zinc ions to the antimicrobial activity of zinc oxide, *Colloids Surf., A*, 2014, **457**, 263–274.

53 N. M. Franklin, N. J. Rogers, S. C. Apte, G. E. Batley, G. E. Gadd and P. S. Casey, Comparative toxicity of nanoparticulate ZnO, bulk ZnO, and $ZnCl_2$ to a freshwater microalga (Pseudokirchneriella subcapitata): the importance of particle solubility, *Environ. Sci. Technol.*, 2007, **41**, 8484–8490.

54 V. Kochkodan and N. Hilal, A comprehensive review on surface modified polymer membranes for biofouling mitigation, *Desalination*, 2015, **356**, 187–207.

55 X. Li, A. Sotto, J. Li and B. Van der Bruggen, Progress and perspectives for synthesis of sustainable antifouling composite membranes containing in situ generated nanoparticles, *J. Membr. Sci.*, 2017, **524**, 502–528.

56 M. Kaneda, X. Lu, W. Cheng, X. Zhou, R. Bernstein, W. Zhang, K. Kimura and M. Elimelech, Photografting Graphene Oxide to Inert Membrane Materials to Impart Antibacterial Activity, *Environ. Sci. Technol. Lett.*, 2019, **6**, 141–147.

57 F. Wang, M. He, K. Gao, Y. Su, R. Zhang, Y. Liu, J. Shen, Z. Jiang and R. Kasher, Constructing membrane surface with synergistic passive antifouling and active antibacterial strategies through organic-inorganic composite modifier, *J. Membr. Sci.*, 2019, **576**, 150–160.
58 C. Leung, Y. Tu, B. Z. Tang and W.-X. Wang, Dissolution Kinetics of Zinc Oxide Nanoparticles: Real-time Monitoring by a Zn^{2+}-specific Fluorescent Probe, *Environ. Sci.: Nano*, 2019, **6**, 2259–2268.
59 H. Jeong, H. Kim and T. Jang, Irrigation water quality standards for indirect wastewater reuse in agriculture: a contribution toward sustainable wastewater reuse in South Korea, *Water*, 2016, **8**, 169.
60 https://www.env.go.jp/en/water/wq/nes.html.
61 J. Yuan, M. I. Van Dyke and P. M. Huck, Identification of critical contaminants in wastewater effluent for managed aquifer recharge, *Chemosphere*, 2017, **172**, 294–301.
62 https://zh.scribd.com/doc/239404461/TI-GB5749-2006-Standards-for-Drinking-Water-Quality.
63 https://www.epa.gov/wqc/national-recommended-water-quality-criteria-organoleptic-effects.
64 https://www2.gov.bc.ca/assets/gov/environment/air-land-water/water/waterquality/wqgs-wqos/approved-wqgs/source_drinking_water_quality_guidelines_bcenv.pdf.
65 B. Wu, J. Wu, S. Liu, Z. Shen, L. Chen, X.-X. Zhang and H.-Q. Ren, Combined effects of graphene oxide and zinc oxide nanoparticle on human A549 cells: bioavailability, toxicity and mechanisms, *Environ. Sci.: Nano*, 2019, **6**, 635–645.

